Letters

Phase Step Control in PLL of DFIG-Based Wind Turbines for Ultrafast Frequency Support

Yini Zhou, *Student Member, IEEE*, Donghai Zhu, *Senior Member, IEEE*, Jiabing Hu, *Senior Member, IEEE*, Xudong Zou, *Member, IEEE*, and Yong Kang, *Fellow, IEEE*

***Abstract*—For doubly-fed induction generator (DFIG)-based wind turbines, this letter proposes a phase step control (PSC) in the phase-locked loop (PLL) to achieve ultrafast frequency support. In the method, a phase angle, associated with the initial frequency differentiation, is appended to the PLL when frequency event occurs. Furthermore, the control parameter of PSC is designed under the constraints of the amplitude of active power. Finally, the proposed method is validated by experiments. The results show that the response time of PSC is less than half of the existing methods, and the frequency metrics are better improved.**

***Index Terms*—Frequency support mechanism, phase-locked loop (PLL), ultrafast response, wind turbine (WT).**

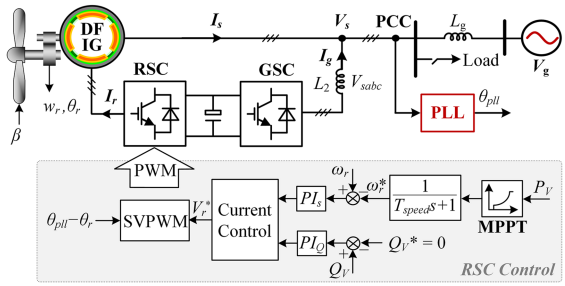

Fig. 1. Control block of the gird-connected DFIG-based WT.

I. Introduction

DRIVEN by the requirements of energy transition, wind power gradually becomes the main power source [1]. However, the existing frequency support methods for wind turbines (WTs) respond to the change of system frequency slowly, difficult in buying time for the primary frequency regulation of the system. To this end, an IEEE standard requires that the response time should not exceed 1 s [2], and China requires it not to exceed 500 ms [3]. Therefore, it is urgent to realize fast frequency support of WTs.

Numerous frequency support methods have been proposed for the doubly fed induction generator (DFIG)-based WT. Additional energy storage control is proposed in [4]; which is efficient and flexible. However, it is costly because of additional hardware. For this reason, many scholars focus on how to release the rotor kinetic energy of the WT to achieve the frequency support. Virtual synchronization generator control can emulate the inertia and damping characteristics of the synchronous generator, but it overturns the original vector control structure, and its transient overcurrent problem has not been well solved [5]. At present, the most common frequency support method is virtual inertia control (VIC), which adds the *df/dt* signal to the outer control loop [6]. However, the response speed of VIC is slow due to the delay of detection, filtering, and communication of the frequency signal. Some scholars have found that modifying the control of the phase-locked loop (PLL) [7], [8] can improve the response speed of frequency support for the WT to some extent. It owns to the reason that the PLL can sense the change of system frequency spontaneously without the communication delay. However, the existing methods about modifying the PLL either reduce the bandwidth of the PLL or introducing a frequency deviation signal by the filter. Therefore, they fail to realize the momentary response to the change of system frequency and still cannot give full play to the rapid adjustment of the PLL to the active power.

In this letter, a phase step control (PSC) in the PLL for DFIG-based WTs is proposed. Once system frequency exceeds deadband, an additional phase angle associated with the initial frequency perturbation will be added to the PLL by PSC. It dramatically improves the response speed to more than twice the existing methods. Besides, the proposed PSC effectively improves the frequency nadir and rate of change of frequency (RoCoF).

II. System Description and Modeling

A. System Description and the Static Model

Fig. 1 illustrates the control block of the grid-connected DFIG-based WT. A DFIG is connected to a grid through the

Received 26 May 2024; revised 7 July 2024; accepted 17 August 2024. Date of publication 23 August 2024; date of current version 12 December 2024. This work was supported in part by the National Natural Science Foundation of China under Grant 52277180 and in part by the Fundamental Research Funds for the Central Universities under Grant YCJJ20242211. *(Corresponding author: Donghai Zhu.)*

The authors are with the State Key Laboratory of Advanced Electromagnetic Technology, School of Electrical and Electronic Engineering, Huazhong University of Science and Technology, Wuhan 430074, China (e-mail: zhouyn@hust.edu.cn; zhudh@hust.edu.cn; j.hu@mail.hust.edu.cn; xdzou@mail.hust.edu.cn; ykang@hust.edu.cn).

Color versions of one or more figures in this article are available at https://doi.org/10.1109/TPEL.2024.3448454.

Digital Object Identifier 10.1109/TPEL.2024.3448454

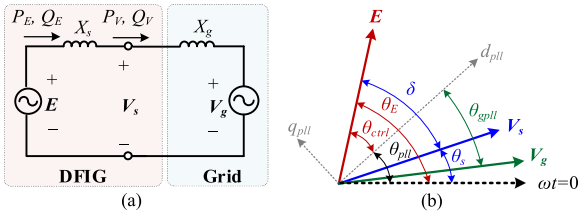

Fig. 2. (a) Equivalent circuit diagram. (b) Vector diagram.

back-to-back converter, where the control structure for the rotor-side converter consists of rotor speed and reactive power outer loops as well as the rotor current inner loop. The research on frequency support belongs to the electromechanical timescale, so the dynamics of the current loop is ignored in this letter.

The internal voltage $\boldsymbol{E}$ of the DFIG is defined as (1) [7], and the output power can be written as (2)

$$\boldsymbol{E} = j\omega_1 L_m \boldsymbol{I_r} = jX_m \boldsymbol{I_r} \tag{1}$$

where ω_1 is the synchronous angular frequency, $\boldsymbol{I_r}$ is the rotor current, and X_m and X_s are the mutual and stator inductances, respectively

$$P_V = (\mathrm{EV}_s \sin\delta)/X_s, \quad Q_V = V_s\left(E\cos\delta - V_s\right)/X_s \tag{2}$$

where V_s is the stator voltage and δ is the angle between $\boldsymbol{E}$ and $\boldsymbol{V_s}$.

The equivalent circuit diagram of the system and its vector relations are shown in Fig. 2. Therein, X_g is the grid inductance.

B. Small-Signal Model for the DFIG-Based WT

Based on (2) and Fig. 2, the small-signal expression for P_V is

$$\hat{P}_V = K_{\theta P}\left(\hat{\theta}_{\mathrm{ctrl}} + \hat{\theta}_{\mathrm{pll}} - \hat{\theta}_s\right) + K_{\mathrm{EP}}\hat{E} \tag{3}$$

where $\hat{\theta}_{\mathrm{pll}} = G_{\mathrm{pll}}\hat{\theta}_s = (K_{\mathrm{ppll}}s + K_{\mathrm{ipll}})/(s^2 + K_{\mathrm{ppll}}s + K_{\mathrm{ipll}})\hat{\theta}_s$. θ_s and θ_{pll} are the of phase angles for $\boldsymbol{V_s}$ and PLL, respectively. θ_{ctrl} is the phase angle between $\boldsymbol{E}$ and d-axis of the PLL. "^" and "0" represent the small signal and the steady value of each variable, respectively. $K_{\theta P} = E_0 V_{s0}\cos\delta_0/X_s$, and $K_{EP} = V_{s0}\sin\delta_0/X_s$.

The small signal for magnitude and the phase angle of $\boldsymbol{E}$ in the phase-locked coordinate system are

$$\begin{cases} \hat{E} = E_{d0}/E_0\hat{E}_d + E_{q0}/E_0\hat{E}_q = K_{dE}\hat{E}_d + K_{qE}\hat{E}_q \\ \hat{\theta}_{\mathrm{ctrl}} = E_{d0}/E_0^2\hat{E}_q - E_{q0}/E_0^2\hat{E}_d = K_{q\delta}\hat{E}_q - K_{d\delta}\hat{E}_d \end{cases}. \tag{4}$$

From Fig. 2, $\boldsymbol{E}$ in the dq-coordinate system can be expressed as

$$\begin{cases} \hat{E}_q = X_m\hat{I}_{rd} = X_m PI_s\left(\hat{\omega}_r - \hat{\omega}_r^*\right) = X_m PI_s\hat{\omega}_{re} \\ \hat{E}_d = -X_m\hat{I}_{rq} = -X_m PI_Q\left(\hat{Q}_V - 0\right) \end{cases} \tag{5}$$

where superscript "$*$" represents the command for each variable.

Combining with (3)–(5), the active power can be written as

$$\hat{P}_V = K_S PI_s\left(\hat{\omega}_r - \hat{\omega}_r^*\right) - K_Q PI_Q\hat{Q}_V + K_{\theta P}\left(\hat{\theta}_{\mathrm{pll}} - \hat{\theta}_s\right) \tag{6}$$

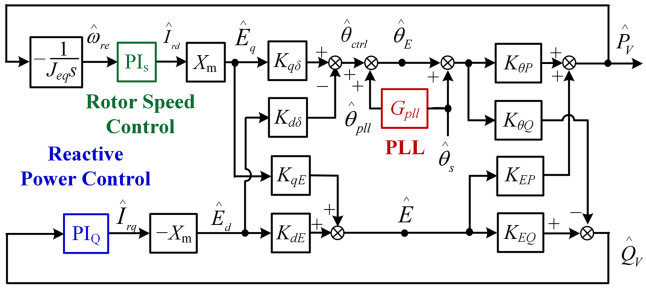

Fig. 3. Small-signal model for the DFIG-based WT.

where $K_S = (K_{\theta P}K_{q\delta} + K_{\mathrm{EP}}K_{qE})X_m$, and $K_Q = (K_{\mathrm{EP}}K_{dE} - K_{\theta P}K_{d\delta})X_m$.

The transfer function between $\hat{P}_V$ and $\hat{\omega}_r - \hat{\omega}_r^*$ is

$$\frac{1}{J_{\mathrm{eq}}s} = -\frac{\hat{\omega}_r - \hat{\omega}_r^*}{\hat{P}_V} = \frac{\left(T_{\mathrm{speed}} + 2H_s\omega_{r0}K_r\right)s + 1 - K_rK_\omega}{\left[2H_s\omega_{r0}s - (K_\omega + K_\beta)\right]\left(T_{\mathrm{speed}}s + 1\right)} \tag{7}$$

where T_{speed} is the rotor speed time constant, and H_s is the inertia constant. $K_r = -1.34P_{V0} + 1.42$, $K_\omega = \rho\pi R^2V^3\partial C_p/(2\partial\omega_r)$, and $K_\beta = \rho\pi R^2V^3\,K_{\mathrm{pitch}}\partial C_p/(2\partial\beta)$. ρ, V, and ω_r are the density of fluid, the wind speed, and the rotor speed, respectively. R is the radius of WT impeller. C_p is the power coefficient, which is a function of the tip-speed ratio λ and the pitch angle β. K_{pitch} is the coefficient of pitch angel control.

In addition, $\hat{Q}_V$ can be obtained from (2)

$$\hat{Q}_V = -K_{\theta Q}\left(\hat{\theta}_{\mathrm{ctrl}} + \hat{\theta}_{\mathrm{pll}} - \hat{\theta}_s\right) + K_{\mathrm{EQ}}\hat{E} \tag{8}$$

where $K_{\theta Q} = E_0V_{s0}\sin\delta_0/X_s$, and $K_{EQ} = V_{s0}\cos\delta_0/X_s$.

According to (5)–(8), the small-signal model for the DFIG-based WT is shown in Fig. 3.

III. Proposed Phase Step Control

A. Frequency Support Mechanism of the WT

It can be seen from (6) and Fig. 3 that the frequency support of DFIG-based WTs can be realized from the following three aspects.

1) *Modify the control of rotor speed:* It is possible to realize frequency support by modifying the control of rotor speed, where the classical method for the WT, called VIC, introduces the *df/dt* signal to the reference of rotor speed or other outer loop [6]. Essentially, VIC changes the rotor speed and releases rotor kinetic energy during frequency event. However, since $J_{\mathrm{eq}}(s)$ is a higher order transfer function with large inertia constants, the response speed is rather slow by modifying the control of rotor speed.
2) *Modify the control of reactive power:* Modifying reactive power controller parameters also has effect on the frequency support of the WT [9]. It owns to the coupling between active power and reactive power in the dynamic process, whereas it is hard to achieve obvious frequency support by modifying the control of reactive power because coupling is generally small.

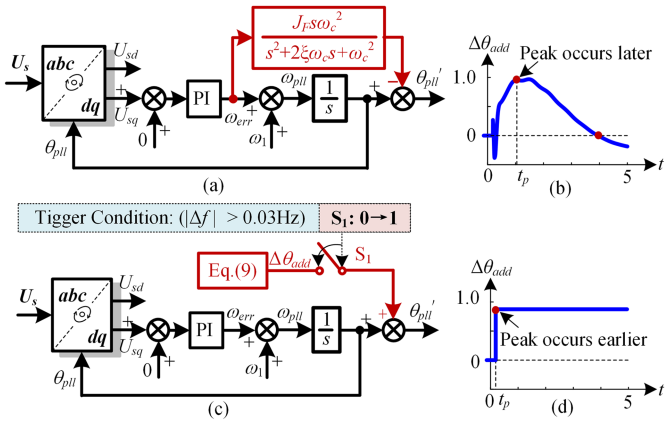

Fig. 4. Frequency support methods by modifying the PLL. (a) Control structure of FFDC. (b) Variation of $\Delta\theta_{\rm add}$ with t in FFDC. (c) Control structure of PSC. (d) Variation of $\Delta\theta_{\rm add}$ with t in PSC.

3) *Modify the control of the PLL:* Modifying controller parameters [7] or the structure of the PLL [8] can achieve frequency support as well. Essentially, they slow down the bandwidth of the PLL or introduces the *df/dt* signal to increase the phase angle difference between $\hat{\theta}_{\rm pll}$ and $\hat{\theta}_s$. Due to no communication delay of frequency signals, modifying the PLL can improve the response speed compared to the above two routes.

B. Proposed PSC

According to the aforementioned analysis, modifying the PLL is a preferable way for realizing fast frequency support. By this way, the feedforward frequency deviation control (FFDC), as shown in Fig. 4(a), is proposed in [8], which introduces the *df/dt* signal to the PLL. After the accident, the system frequency drops, and *df/dt* is largest at the beginning in theory. Since the differentiation of frequency is difficult to realize in practice, it is usually in series with a low-pass filter, causing the maximum $|\text{RoCoF}|_{\max}$ to lag. It will take a long time for $\Delta\theta_{\rm add}$, namely, $\hat{\theta}_{\rm pll} - \hat{\theta}_s$ in FFDC, to arrive at the maximum value in Fig. 4(b). Therefore, it can be seen from Fig. 3 that $\hat{P}_V$ will reach its maximum value rather slowly as well.

To avoid the slow growth of active power caused by the slow increase of $\Delta\theta_{\rm add}$, a PSC shown in Fig. 4(c) is proposed, where the phase step occurs at the moment the disturbance is detected. There is no low-pass filter delay, and the response speed can be ultrafast. By this way, an additional angle $\Delta\theta_{\rm add}$ in (9) will be added to $\theta_{\rm pll}$' once frequency deviation Δf exceeds limit, where $\Delta\theta_{\rm add}$ of PSC can change momentarily like Fig. 4(d). Therefore, $\hat{P}_V$ can reach the maximum value momentarily. $\Delta\theta_{\rm add}$ depends on the initial change of frequency $\Delta f/\Delta t$ for accommodating different size of load disturbance scenarios, and $\theta_{\rm pll}$' will participate in coordinate transformation

$$\Delta\theta_{\rm add} = K(f_0 - f_1)/(t_1 - t_0) = -K\Delta f/\Delta t \tag{9}$$

where K is the proportional coefficient. f_0 is the steady-state frequency before the accident. t_0 is the initial moment of the accident. When the initial |RoCoF| exceeds the limit, f_i and t_i will be recorded as the steady-state frequency f_0 and the initial moment t_0 of the accident, respectively. t_1 and f_1 are the moment and the frequency when system frequency starts to exceed the limit, respectively. "Δ" represents the change of each variable.

C. Parameter Design

An IEEE standard proposed that the temporary increase of active power is required to be equal to at least 5% of the rated power of WTs [2]. It is worth noting that the change of active power ΔP_V will change abruptly after $\Delta\theta_{\rm add}$ is introduced, and then, speed control will gradually regulate the active power back to its steady value. To this reason, the initial change of the active power ΔP_{V1} at $t = t_1$ is generally the maximum value, and it is desired to be larger than 0.05 p.u. For obtaining a proper $\Delta\theta_{\rm add}$ to meet the requirement, the controller parameter K is needed to be designed.

Since the fact that $\Delta\theta_{\rm add}$ may not be very tiny, the small-signal model in Fig. 3 is no longer applicable, and the change of ΔP_{V1} needs to be deduced with the change of the phase-locked coordinate system, where all the variables are normalized. Based on (2), the change of power with the disturbance of $\Delta\theta_{\rm add}$ can be obtained as

$$\begin{cases} \Delta P_{V1} = \left[\begin{array}{l}\sqrt{(E_{d0}+\Delta E_{d1})^2 + E_{q0}^2}\,(V_{s0}+\Delta V_{s1}) \\ \times \sin(\delta_0 + \Delta\theta_{\rm ctrl1} + \Delta\theta_{\rm add})\end{array}\right] \Big/ X_s - P_{V0} \\ \Delta Q_{V1} \\ = \left[\begin{array}{l}\sqrt{(E_{d0}+\Delta E_{d1})^2 + E_{q0}^2}\,(V_{s0}+\Delta V_{s1}) \\ \times \cos(\delta_0 + \Delta\theta_{\rm ctrl1} + \Delta\theta_{\rm add}) - (V_{s0}+\Delta V_{s1})^2\end{array}\right] \Big/ X_s - Q_{V0} \end{cases} \tag{10}$$

where ΔP_{V1}, ΔQ_{V1}, ΔE_{d1}, ΔV_{s1}, and $\Delta\theta_{\rm ctrl1}$ are the changes of P_{V1}, Q_{V1}, E_d, V_s, and $\theta_{\rm ctrl}$ at t_1, respectively.

According to Fig. 2, the change of V_s at t_1 can be obtained as

$$\begin{cases} \Delta V_{sd1} = (X_g\Delta E_{d1} + X_s\Delta V_{gd1})/(X_g + X_s) \\ \Delta V_{sq1} = (X_g\Delta E_{q1} + X_s\Delta V_{gq1})/(X_g + X_s) \\ \qquad = \frac{X_s}{X_g+X_s}\Delta V_{gq1} = -\tan(\Delta\theta_{\rm add})(\Delta V_{sd1} + V_{sd0}) \\ \Delta V_{s1} = \sqrt{(V_{sd0}+\Delta V_{sd1})^2 + (V_{sq0}+\Delta V_{sq1})^2} - V_{s0} \end{cases} \tag{11}$$

where ΔV_{gd1} and ΔV_{gq1} are the changes of V_{gd} and V_{gq} at t_1, respectively. $V_{sd0} = 1$, and $V_{sq0} = 0$. From Fig. 3, ΔE_{q1} cannot response to $\Delta\theta_{\rm pll}$' momentarily and $\Delta E_{q1} = 0$ due to the large inertia constants of $J_{\rm eq}$(s). ΔE_{d1} can response momentarily because of the proportional coefficient of the reactive power controller, and $\Delta E_{d1} = -K_{pQ}X_m\Delta Q_{V1}$.

From (11) and Fig. 2, ΔV_{gd1}, ΔV_{gq1}, and $\Delta\theta_{\rm ctrl1}$ with the disturbance of $\Delta\theta_{\rm add}$ can be derived as

$$\begin{cases} \Delta V_{gd1} = \\ \pm\sqrt{1 - \left(V_{gq0} - \frac{X_g+X_s}{X_s}\tan(\Delta\theta_{\rm add})(\Delta V_{sd1} + V_{sd0})\right)^2} \\ -V_{gd0} \\ \Delta V_{gq1} = -\frac{X_g+X_s}{X_s}\tan(\Delta\theta_{\rm add})(\Delta V_{sd1} + V_{sd0}) \\ \Delta\theta_{\rm ctrl1} = \text{actran}[E_{q0}/(E_{d0}+\Delta E_{d1})] - \text{actran}(E_{q0}/E_{d0}) \end{cases} \tag{12}$$

where the sign of the first equation in (12) takes "+" when $V_{gd0} + \Delta V_{gd1} > 0$, otherwise takes "-."

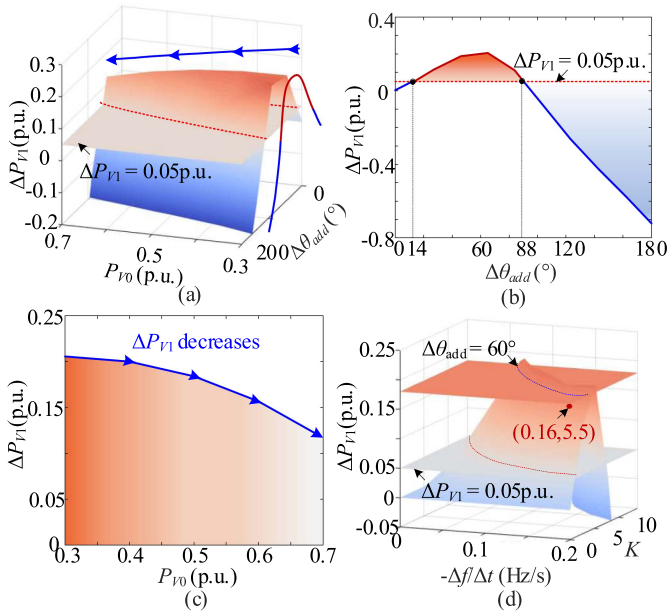

Fig. 5. Design constraints for parameter K. (a) 3-D diagram of ΔP_{V1} as a function of P_{V0} and $\Delta\theta_{\text{add}}$. (b) Change of ΔP_{V1} with $\Delta\theta_{\text{add}}$. (c) Change of ΔP_{V1} with ΔP_{V0}. (d) 3-D diagram of ΔP_{V1} as a function of K and $-\Delta f/\Delta t$.

Combining (9)–(12) and the various operating points of the WT, the 3-D diagram of ΔP_{V1} as a function of P_{V0} and $\Delta\theta_{\text{add}}$ is shown in Fig. 5(a). To clearly show the analysis results, the changes of ΔP_{V1} with $\Delta\theta_{\text{add}}$ and P_{V0} are shown in Fig. 5(b) and (c), respectively, where P_{V0} is 0.55 p.u. in Fig. 5(b), and $\Delta\theta_{\text{add}}$ is 50.1° in Fig. 5(c).

From Fig. 5(a) and (b), ΔP_{V1} first increases and then decreases as $\Delta\theta_{\text{add}}$ increases. What is more, when $\Delta\theta_{\text{add}}$ is very large, the situation that $\Delta P_{V1} < 0$ will even occur. Taking $P_{V0} = 0.55$ p.u. in Fig. 5(b) as an example, $14° < \Delta\theta_{\text{add}} < 88°$ should be satisfied to guarantee $\Delta P_{V1} > 0.05$ p.u. In addition, as illustrated in Fig. 5(c), ΔP_{V1} decreases as P_{V0} increases, and the optional range of $\Delta\theta_{\text{add}}$ in Fig. 5(a) decreases as P_{V0} increases. Therefore, $\Delta\theta_{\text{add}} < 60°$ is recommended in this letter to satisfy the requirement of ΔP_{V1} as far as possible under different operating conditions.

Furthermore, based on (9), the 3-D diagram of ΔP_{V1} as a function of K and $-\Delta f/\Delta t$ is shown in Fig. 5(d). Finally, K can be chosen in the region between the two dashed lines. Because different sizes of load disturbances often occur in the system, K should be adaptable in a wide range of $\Delta f/\Delta t$. Therefore, the value of K should be chosen moderately in the region between the two dashed lines of Fig. 5(d).

IV. Experimental Validations

To verify the proposed PSC, a 100×1.5 MW grid-connected DFIG-based WT system, as shown in Fig. 1, is constructed on the hardware-in-the-loop experiment platform. A load is put into the system at 50 s to simulate the frequency perturbation event. The detailed description of the platform is given in [10], and parameters of the DFIG are given in Table III of the Appendix. Since $-\Delta f/\Delta t$ is 0.08–0.16 Hz/s in this letter, K can be designed as 5.5 in PSC.

TABLE I
Frequency Support Performance Metrics for Different Methods

Case	Method	Response time (ms)	f_{nadir} (Hz)	$\lvert\text{RoCoF}\rvert_{\max}$ (Hz/s)
A	w/o control	\	49.053	0.4062
	VIC [6]	960	49.130	0.3318
	FFDC [8]	915	49.108	0.3321
	Proposed PSC	248	49.234	0.3275
B	w/o control	\	49.053	0.4059
	VIC [6]	878	49.138	0.3269
	FFDC [8]	823	49.076	0.3074
	Proposed PSC	303	49.222	0.2917
C	w/o control	\	49.526	0.2023
	VIC [6]	897	49.554	0.1739
	FFDC [8]	836	49.551	0.1644
	Proposed PSC	387	49.621	0.1596

Note: Response time in this letter is the time taken by the active power to get to 90% of its peak value.

A. Effect of Different Control Parameter

Fig. 6 shows the effect of different control parameters on the power response of PSC, where load disturbance is 100 MW and $-\Delta f/\Delta t$ is 0.16Hz/s. When $K = 1$, $\Delta\theta_{\text{add}} = 9.1°$, and it is smaller than the lower limit of $\Delta\theta_{\text{add}}$. Therefore, ΔP_{V1} is only 0.037 p.u. in Fig. 6(a), which is smaller than 0.05 p.u. When $K = 5.5$, $\Delta\theta_{\text{add}} = 50.1°$, and it is in the range of $14° < \Delta\theta_{\text{add}} < 88°$. Therefore, ΔP_{V1} in Fig. 6(b) is 0.161 p.u., satisfying the requirement of $\Delta P_{V1} > 0.05$ p.u. When K is further increased to 12, that is, $\Delta\theta_{\text{add}} = 110.1°$, the active power in Fig. 6(c) decreases instead of increasing and $\Delta P_{V1} = -0.132$ p.u. All in all, it proves the analysis in Section III-C.

B. Effect of Different Operating Conditions and Load Disturbances

To examine the validity and the adaptability of the PSC under different operating conditions and load disturbances, the following experiments of Cases A–C are performed. In addition, the proposed PSC is compared with VIC [6] and FFDC [8].

1) Case A: Wind Speed is 10 m/s, and the Size of Load Disturbance is 100 MW: Fig. 7 shows the results of different frequency support methods. In Case A, the maximum active power increments ΔP_{Vmax} of these frequency support methods are controlled to the same, so as to compare the response speed and frequency support capability of them. From Fig. 7(a), once frequency exceeds the deadband, PSC can respond to the drop of frequency momentarily, and response time is only 248 ms, which is much faster than VIC and FFDC, and the support time of PSC is about twice that of VIC and FFDC methods. Therefore, f_{nadir} of PSC is much higher than that of VIC and FFDC, which can be seen in Fig. 7(b). In addition, it can be seen in Fig. 7(c) that $\lvert\text{RoCoF}\rvert_{\max}$ of PSC is smaller than those of VIC and FFDC. Thus, PSC is superior in response speed and frequency support.

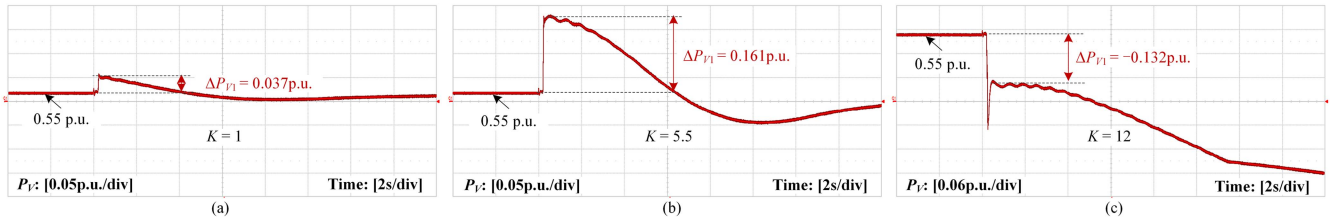

Fig. 6. Effect of control parameter K. (a) $K = 1$. (b) $K = 5.5$. (c) $K = 12$.

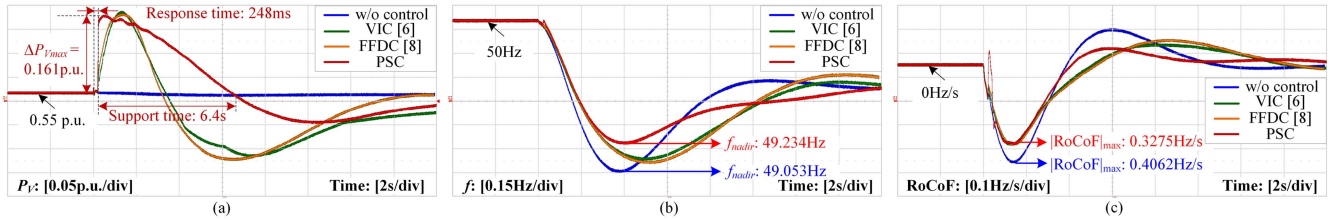

Fig. 7. Results for Case A. (a) Power response of the WT. (b) System frequency. (c) RoCoF of the system.

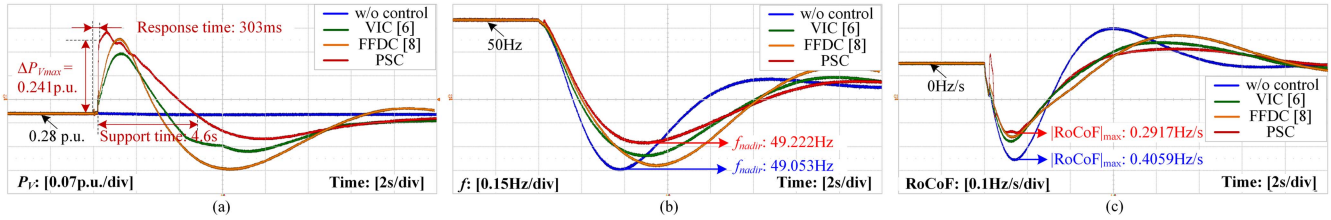

Fig. 8. Results for Case B. (a) Power response of the WT. (b) System frequency. (c) RoCoF of the system.

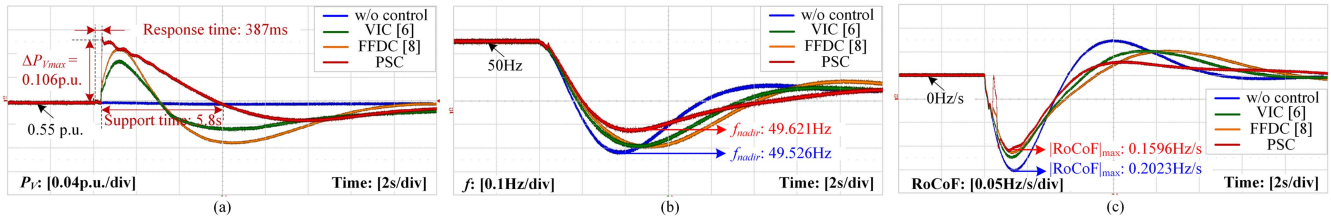

Fig. 9. Results for Case C. (a) Power response of the WT. (b) System frequency. (c) RoCoF of the system.

2) Case B: Wind Speed is 8 m/s, and the Size of Load Disturbance is 100 MW: Fig. 8 shows the results of different frequency support methods under a lower wind speed. Comparing with Case A, it can be seen from Fig. 8(a) that the lower the wind speed, the higher the power increment of the PSC with the same control parameters. It proves the analysis in Section III-C. In this case, the response speed of PSC is more than twice that of VIC and FFDC, and the support time of PSC is longer than that of VIC and FFDC methods. Therefore, the frequency nadir of PSC in Fig. 8(b) and $|\text{RoCoF}|_{\max}$ in Fig. 8(c) are better improved. It indicates that the designed parameter K makes PSC adaptable in different operating conditions.

3) Case C: Wind Speed is 10 m/s, and the Size of Load Disturbance is 50 MW: Fig. 9 shows the results of different frequency support methods under a smaller load disturbance. Comparing with Case A, the active power increments of the all frequency support methods in Fig. 9(a) decrease, but the increment of PSC is still the largest, the support time is the longest, and the response speed is the fastest. Therefore, the frequency nadir of PSC in Fig. 9(b) and $|\text{RoCoF}|_{\max}$ in Fig. 9(c) are better improved in this case as well. It indicates that the designed parameter K makes PSC adaptable in different load disturbance conditions as well.

To clearly illustrate the experiment results, the frequency support performance metrics are listed in Table I.

V. Discussion

To compare the advantages and limitations of different frequency support methods, VIC, FFDC, and PSC are compared in terms of implementation complexity, response time, and support performance. For implementation complexity, both the VIC and

TABLE II
ADVANTAGES AND LIMITATIONS OF DIFFERENT METHODS

Method	Implementation	Response speed	Support for $\|\text{RoCoF}\|_{\max}$	Support for f_{nadir}
VIC [6]	Easy	Slow	Normal	Strong
FFDC [8]	Easy	Fast	Strong	Normal
PSC	Very easy	Ultrafast	Very Strong	Very Strong

the FFDC require filtering of the *df/dt* signal, but PSC does not need. Therefore, PSC is very easy to implement, and the response speed is ultrafast. The response speed of FFDC is faster than that of the VIC since the former introduces the *df/dt* signal in the PLL rather than the outer loop. Since the response speed of PSC is the fastest, the support of PSC for $|\text{RoCoF}|_{\max}$ is the strongest, followed by FFDC and VIC. In addition, based on the results of the aforementioned experiments, it can be seen that the support time of PSC is the longest, followed by VIC and FFDC. Thus, the support of PSC for f_{nadir} is stronger than that of VIC and FFDC. Finally, the advantages and limitations of different frequency support methods are compared in Table II.

The PSC is also applicable to other new energy devices as they all adopt the PLL. In addition, the cooperation of multiple WTs and the balance in the speed recovery stage between the secondary frequency drop and the rotor speed recovery time will be investigated in the future.

VI. CONCLUSION

This letter proposes a PSC in the PLL of DFIG-based WTs for ultrafast frequency support. The main conclusions are summarized as follows.

1) WT's frequency support can be realized by modifying the control of rotor speed, reactive power, or PLL. However, either the response is slow or the frequency support is weak for the first two routes.
2) Changing the phase of the PLL directly can affect power dynamics swiftly, allowing for ultrafast frequency support. The PSC can more than double the response speed, and it can provide with the better frequency support.
3) As the control parameter K of PSC increases, $\Delta\theta_{\text{add}}$ increases, but the output power first increases and then decreases. To meet the requirements for the amplitude of the temporary increase of active power, the design of K should ensure that $\Delta\theta_{\text{add}}$ is within the appropriate range.

APPENDIX

TABLE III
PARAMETERS OF THE 1.5-MW DFIG-BASED WT

Description	Symbol	Value
Rated power	P_N	1.5 MW
Rated stator voltage	V_{SN}	690 V
Grid frequency	f_g	50 Hz
DC-link voltage	U_{dc}	1200 V
Turns radio	N_s/N_r	0.4
Stator resistance	R_s	0.023 p.u.
Rotor resistance	R_r	0.016 p.u.
Magnetizing inductance	L_m	2.9 p.u.
Stator leakage inductance	L_{ls}	0.18 p.u.
Rotor leakage inductance	L_{lr}	0.16 p.u.
DC bus capacitor	C_{dc}	10000 μF
Controller of rotor speed	K_{ps}, K_{is}	1, 0.6
Controller of reactive power	K_{pQ}, K_{iQ}	2, 0.2

REFERENCES

[1] Y. Zhou et al., "Magnitude-phase characteristics analysis of inertia for DFIG-based wind turbines," *IEEE Trans. Power Electron.*, vol. 39, no. 10, pp. 12336–12348, Oct. 2024.
[2] *IEEE Standard for Interconnection and Interoperability of Inverter-Based Resources (IBRs) Interconnecting With Associated Transmission Electric Power Systems*, IEEE Standard 2800-2022, 2022, pp. 1–180.
[3] L. Li, D. Zhu, X. Zou, J. Hu, Y. Kang, and J. M. Guerrero, "Review of frequency regulation requirements for wind power plants in international grid codes," *Renewable Sustain. Energy Rev.*, vol. 187, 2023, Art. no. 113731.
[4] J. Fang, Y. Tang, H. Li, and X. Li, "A battery/ultracapacitor hybrid energy storage system for implementing the power management of virtual synchronous generators," *IEEE Trans. Power Electron.*, vol. 33, no. 4, pp. 2820–2824, Apr. 2018.
[5] H. Wu, X. Wang, and L. Zhao, "Design considerations of current-limiting control for grid-forming capability enhancement of VSCs under large grid disturbances," *IEEE Trans. Power Electron.*, vol. 39, no. 10, pp. 12081–12085, Oct. 2024.
[6] J. Fang, P. Lin, H. Li, Y. Yang, and Y. Tang, "An improved virtual inertia control for three-phase voltage source converters connected to a weak grid," *IEEE Trans. Power Electron.*, vol. 34, no. 9, pp. 8660–8670, Sep. 2019.
[7] W. He, X. Yuan, and J. Hu, "Inertia provision and estimation of PLL-based DFIG wind turbines," *IEEE Trans. Power Syst.*, vol. 32, no. 1, pp. 510–521, Jan. 2017.
[8] D. Zhu, X. Guo, B. Tang, J. Hu, X. Zou, and Y. Kang, "Feedforward frequency deviation control in PLL for fast inertial response of DFIG-based wind turbines," *IEEE Trans. Power Electron.*, vol. 39, no. 1, pp. 664–676, Jan. 2024.
[9] L. Sun and X. Zhao, "Impacts of phase-locked loop and reactive power control on inertia provision by DFIG wind turbine," *IEEE Trans. Energy Convers.*, vol. 37, no. 1, pp. 109–119, Mar. 2022.
[10] D. Zhu, Z. Wang, Y. Ma, J. Hu, X. Zou, and Y. Kang, "Hybrid LVRT control of doubly-fed variable speed pumped storage to shorten crowbar operational duration," *IEEE Trans. Power Electron.*, early access, doi: 10.1109/TPEL.2024.3435063.